AIP Publishing

This manuscript was accepted by Appl. Phys. Lett. Click here to see the version of record.

1 **Formation and Properties of InGaN QDs: Influence of Substrates**

2 A. S. Chang[1], J. C. Walrath[2], T. Frost[3], C. Greenhill[4], J. Occena[4], A. Hazari[3], P. Bhattacharya[3],
3 and R. S. Goldman[2,4*]
4 [1]Department of Materials Science and Engineering, Northwestern University, Evanston, Illinois
5 60208, USA
6 [2]Department of Physics, [3]Department of Electrical and Computer Engineering, [4]Department of
7 Materials Science and Engineering, University of Michigan, Ann Arbor, Michigan 48109, USA

8 11/30/18

ACCEPTED MANUSCRIPT

9 **Abstract**

10 We examine the formation and properties of InGaN quantum dots (QDs) on free-standing GaN
11 and GaN/sapphire templates, with and without buried InGaN/GaN QD superlattices (SLs). We use
12 scanning tunneling microscopy and scanning tunneling spectroscopy to image the QDs and
13 measure their electronic states. As the number of layers preceding the QDs increase (i.e. increasing
14 substrate complexity), the total QD density increases. For free-standing GaN, STM reveals a
15 mono-modal QD-size-distribution, consistent with a limited density of substrate threading
16 dislocations serving as heterogeneous nucleation sites. For GaN/sapphire templates, STM reveals
17 a bimodal QD-size-distribution, presumably due to the nucleation of additional ultra-small InN-
18 rich QDs near threading dislocations. For multi-period QD SLs on GaN/sapphire templates, an
19 ultra-high density of QDs, with a mono-modal size distribution is apparent, suggesting that QD
20 nucleation is enhanced by preferential nucleation at strain energy minima directly above buried
21 QDs. We discuss the relative influences of strain fields associated with threading dislocations and
22 buried QD SLs on the formation of InGaN QDs and their effective band gaps.

AIP Publishing

This manuscript was accepted by Appl. Phys. Lett. Click here to see the version of record.

1 *Corresponding Author: rsgold@umich.edu

2 In recent years, InGaN alloys have been successfully implemented in visible light emitters
3 and detectors.[1,2] Typically, the performance of InGaN quantum-well based devices is hindered by
4 misfit-strain-induced and spontaneous piezoelectric polarizations, both of which lead to the spatial
5 separation of electron and hole wavefunctions.[3] To minimize the influence of strain-induced and
6 spontaneous polarizations, several alternative configurations have been proposed.[4,5] For example,
7 strain-free InGaN-based nanowires on silicon have been demonstrated for light-emitters operating
8 from the near-IR to the visible ranges.[6] In addition, reduced spontaneous polarizations are
9 predicted in ellipsoidal-shaped InGaN quantum dots (QDs), which have non- or semi-polar
10 surfaces.[7] Indeed, InGaN-based QD heterostructures have been utilized for light-emitters
11 operating from blue to red emission ranges.[8,9] For conventional III-Vs, such as InAs/GaAs,
12 homogeneous nucleation of QDs is typically observed.[10] For QD superlattices (SLs), QD
13 nucleation often occurs preferentially at strain energy minima directly above buried QDs, leading
14 to vertical alignment of QDs, with an increase or decrease in the regularity of QD spacing.[11,12] For
15 GaN-based systems, threading dislocations have been reported to provide residual stresses that
16 serve as heterogeneous QD nucleation sites.[13] In the case of InGaN/GaN QD SLs, conflicting
17 trends of a constant or an increase in QD density with increasing the number of QD SLs have been
18 reported.[12,14,15] Here, we report on the formation of InGaN QDs, with an emphasis on the role of
19 the substrate on QD nucleation and growth. We use scanning tunneling microscopy (STM) and
20 scanning tunneling spectroscopy (STS) to image the InGaN QDs and measure their electronic
21 states. As the number of layers which precede the QDs increases (i.e. increasing substrate
22 complexity), the total QD density increases. We discuss the relative influences of strain fields

ACCEPTED MANUSCRIPT

AIP Publishing
This manuscript was accepted by Appl. Phys. Lett. Click here to see the version of record.

1 associated with threading dislocations and buried QD SLs on the formation of InGaN QDs and
2 their corresponding band offsets.

3 For these investigations, InGaN QDs were deposited on GaN using molecular-beam
4 epitaxy (MBE) using solid Ga and In sources, with an ultra-high purity N_2 plasma source. Single-
5 layer InGaN QDs were grown on free-standing n^+ GaN (0001) substrates, with root mean square
6 (RMS) roughness < 0.5nm and etch pit densities < $5x10^4/cm^2$.[16] In addition, single-layer InGaN
7 QDs and three-period InGaN/GaN QD SLs were grown on GaN/AlN/sapphire templates, with
8 RMS roughness < 1.0 nm and etch pit densities < $10^9/cm^2$.[17,18] As shown in the sample cross-
9 sections in Fig. 1, we term the QDs as "QD-free-standing" and "QD-template", and the 3-period
10 QD SLs as "multi-QD-template".

11 In all cases, n+ GaN buffers and 12 nm spacers, Si-doped at ~$5x10^{18}/cm^3$, were grown at
12 710 °C with a Ga flux of $2.2x10^{-7}$ Torr, N_2 flow rate of 0.66 sccm, and N_2 plasma power of 350
13 W. For the QDs, 8 MLs of InGaN were deposited at 540 °C, with a Ga flux of $4x10^{-8}$ Torr, In flux
14 of $9x10^{-8}$ Torr, N_2 flow rate of 1.33 sccm, and N_2 plasma power of 420 W. The targeted "global"
15 indium fraction for the InGaN layers was x_{In}=0.4, and atom-probe tomography (APT) of similar
16 samples suggest x_{In}~0.04 in the wetting layer.[8,14]

17 For these samples, high-resolution X-ray diffraction data were collected as a function of
18 azimuthal angle, revealing negligible (i.e. <0.5°) epilayer rotation about an in-plane axis (i.e.
19 epilayer tilt). Therefore, the vicinality of the starting surfaces is likely to be negligible. We note
20 that plastic relaxation due to threading dislocation bending at the interface is unlikely due to the
21 negligible substrate offcut, the low QD growth temperatures (540 °C), and the low total thickness
22 of WL+QD (8ML or 4.2 nm). Furthermore, it was recently reported that plastic relaxation of
23 InGaN grown on free standing GaN is dislocation nucleation-limited, with minimal

ACCEPTED MANUSCRIPT

AIP Publishing

This manuscript was accepted by Appl. Phys. Lett. Click here to see the version of record.

1 misfit/threading dislocation interactions.[19] Since the formation of QDs leads to significant elastic
2 strain relaxation, the strain-induced polarization fields are expected to be minimal. Furthermore,
3 since the QDs are ellipsoid-shaped, with portions of non-(0001) oriented surfaces, the spontaneous
4 polarization fields are also expected to be minimal.

5 Prior to plan-view STM, the samples were transferred from the MBE to the STM chamber
6 via a mobile transfer system (~10^{-2} Torr), with ambient exposure limited to < 1 minute. Both STM
7 and STS were performed with commercially-available W and Pt/Ir tips, cleaned in-situ by electron
8 bombardment. STS measurements were performed using the variable tip-sample separation
9 method.[20] All images were obtained with a sample bias voltage of -3.5 V and constant tunneling
10 current of 200 pA. We examined several STM images spanning > 1 μm^2, and acquired STS spectra
11 in the vicinity of InGaN QDs and surrounding InGaN wetting layers. Furthermore,
12 photoluminescence (PL) measurements of an unintentionally-doped heterostructure, consisting of
13 7-period QD superlattices, revealed 2.0 eV emission at room temperature.

14 Figure 2 shows (a) a schematic and (b) a large-scale STM image of QD-free-standing, as
15 well as large-scale STM images of (d) QD-template and (e) multi-QD-template. Within each QD
16 SL, bright and dark regions corresponding to InGaN QDs and WL are apparent. For example, in
17 Fig. 2(b), a nanostructure with ~100 nm length, ~50 nm width, and ~6 nm height, resembling a
18 quantum dash or two adjacent InGaN QDs,[21] is apparent. In Figs. 2(d) and 2(e), example QDs are
19 labelled with white arrows. To determine the QD densities and size distributions, we use a
20 threshold method to determine the percentage of QDs with diameters within a specific range.
21 Image regions with tip-heights above 5x the RMS tip-heights of the substrate were identified as
22 QDs. We fit the frequency as a function of QD diameter with a Gaussian distribution and used the
23 maximum-likelihood-estimation method to obtain the most probable QD diameter, i.e. mean QD

ACCEPTED MANUSCRIPT

AIP Publishing

This manuscript was accepted by Appl. Phys. Lett. Click here to see the version of record.

1 diameter.[22] The resulting QD-size-distributions are presented in Fig. 2 for (c) QD-free-standing
2 and (f) QD-template and multi-QD-template. As will be discussed in more detail below, using the
3 QD densities and sizes from STM and the local composition measurements from STS, the indium
4 incorporation is equivalent for all cases.

5 For QD-free-standing, the QD density is $1.6x10^{10}/cm^2$, with mean QD diameter of 17±3
6 nm. Since the substrate etch pit density is $< 10^5/cm^2$, an insufficient density of QD nucleation sites
7 is provided by the substrate dislocations. Instead, homogeneous nucleation, followed by growth
8 via coalescence, is expected.[13] Since there is one process for QD nucleation and growth, the
9 distribution of QD sizes is monomodal.

10 For QD-template, a bimodal distribution of QD diameters, with most probable values of
11 23±1 nm and 3±1 nm, is observed. The corresponding densities of large and ultra-small QDs, are
12 $1.7x10^{11}/cm^2$ and $5x10^{10}/cm^2$, respectively. In this case, the RMS roughness and miscut of the
13 template substrate are also negligible, but the etch pit density is four orders of magnitude higher
14 than that of the free-standing substrate. We therefore hypothesize that In atom clusters are
15 heterogeneously nucleated near threading dislocations to form ultra-small QDs.[23] As the ultra-
16 small QDs grow in size, the interaction energy between In clusters and threading dislocations
17 saturates, leading to a limited QD size. In addition to the ultra-small QDs, large QDs nucleate
18 homogeneously away from the threading dislocations, followed by continuous growth via
19 coalescence. Since the QDs near and away from the threading dislocations have different processes
20 for QD nucleation and growth, the distribution of QD sizes is bimodal.

21 Finally, for multi-QD-template, the QD density is $1.8x10^{12}/cm^2$, with mean QD diameter
22 of 5±3 nm. Since the distribution of QD diameters is mono-modal, with a significantly higher
23 mean diameter than those grown directly on the templates, a heterogeneous nucleation mechanism

ACCEPTED MANUSCRIPT

AIP Publishing

This manuscript was accepted by Appl. Phys. Lett. Click here to see the version of record.

ACCEPTED MANUSCRIPT

is likely. The QD nucleation and growth most likely occur preferentially at strain energy minima directly above buried QDs.[11] Subsequently, growth via coalescence is expected. There is again one process for QD nucleation and growth, and the distribution of QD sizes is monomodal.

In Fig. 3, normalized conductance versus sample voltage collected from the (a) QD-free-standing, (b) QD-template, and (c) multi-QD-template are presented. In all cases, the sample voltage corresponds to the energy relative to the Fermi level. STS data was collected both in the vicinity of the InGaN QDs and in the nearby 2D InGaN wetting layers. For the InGaN WL, STS spectra, shown as the solid-line spectra in Figs. 3(a) – 3(c), reveal well-defined band edges with effective band gap values of 3.4±0.1 eV. On the other hand, for similarly grown 2D wetting layers, the indium fraction has been estimated as x_{In}=0.04. Using a quadratic deviation from a linear interpolation of binary InN and GaN band gaps of 0.69 eV and 3.4 eV, with a bowing parameter of 2.1 eV,[24] the estimated x_{In} of 0.04 leads to a band gap of 3.2 eV. The higher effective band gap value determined by STS is due to tip-induced band bending. Thus, to correct all other STS data for tip-induced band bending, we multiply each effective band gap value by a correction factor based upon that of the wetting layer, i.e. 3.2/3.4 = 0.94.

In the vicinity of the InGaN QDs, the effective band gaps are lower than those of InGaN WL. Since both strain-induced and spontaneous polarization fields are expected to be minimal in the InGaN QDs,[8] we attribute the local variations in effective band gaps to local variations in the indium composition. To quantify the local indium composition, we consider the influence of tip-induced band-bending, described above, plus the effects of quantum confinement. In particular, we consider a pancake-shaped QD, with an effective height of 1/3 of the QD diameter. Assuming one-dimensional confinement along the growth direction, with literature values for the InGaN/GaN band offsets and effective masses,[25,26,27] we estimate the effective bandgaps as

AIP Publishing

This manuscript was accepted by Appl. Phys. Lett. Click here to see the version of record.

1 $$E_g^*(effective) = E_g(STS) - \frac{\hbar\pi^2}{2}\left(\frac{1}{m_e} + \frac{1}{m_h}\right)\left(\frac{3}{d}\right)^2,$$

2 where d is the diameter of the QD, and $m_e^* = 0.2m_e$ and $m_h^* = 1.3m_h$ are the electron and hole
3 effective masses for GaN, respectively.

4 We now discuss the effective bandgaps in the vicinity of QD-free-standing. In Fig. 3(a),
5 the normalized conductance versus sample bias voltage is plotted for the center, inner edge, and
6 outer edge of an InGaN QD, in comparison with region of InGaN WL. Positions where STS spectra
7 were collected are indicated by circular symbols in Fig. 2(b). Effective band gaps of 2.1±0.1 eV,
8 2.9±0.1 eV, and 3.2±0.1 eV, corresponding to local indium compositions of 0.28, 0.11, and 0.04,
9 are observed at the center, inner edge, and outer edge of the InGaN QD, respectively. The
10 variations in the local indium composition, with the highest values near the QD center, are
11 consistent with scanning transmission electron microscopy reports on InGaN/GaN QDs.[28] In
12 addition, similar trends have been reported for InAs/GaAs QD systems and attributed to lateral
13 gradients in x_{In}.[29]

14 For QD-template, the normalized conductance versus sample bias voltage is plotted in Fig.
15 3(b) for the center of the large QD, the edge of the large QD, and the center of the ultra-small QD,
16 in comparison with a region of InGaN WL. In this case, effective band gaps of 2.5±0.1 eV, 3.1±0.1
17 eV, and 1.7±0.1 eV, corresponding to local indium compositions of 0.21, 0.06, and 0.44, are
18 observed at the center of the large QD, edge of the large QD, and center of the ultra-small QD,
19 respectively. For QD-template, the sum of the QD densities for large and ultra-small QDs is
20 $2.2\text{x}10^{11}/\text{cm}^2$, an order of magnitude higher than the QD density of QD-free-standing, most likely
21 due to the higher density of threading dislocations in the GaN/sapphire than in the free-standing
22 GaN templates.[14,15] For QD-template, we hypothesize that ultra-small InN-rich QDs were
23 heterogeneously nucleated near the threading dislocations, consistent with predictions of In-rich

ACCEPTED MANUSCRIPT

AIP Publishing

This manuscript was accepted by Appl. Phys. Lett. Click here to see the version of record.

1 cluster formation near threading dislocations during InGaN alloy growth.[23]

2 Finally, we discuss the effective band gaps in the vicinity of multi-QD-template. The
3 normalized conductance versus sample bias voltage is plotted in Fig. 3(c) for the center and edge
4 of the InGaN QD, in comparison with a region of InGaN WL. Here, effective band gaps of 2.4±0.1
5 eV and 3.2±0.1 eV, corresponding to local indium compositions of 0.23 and 0.04, are observed at
6 the center and edge of the InGaN QD, respectively. We note that the estimated local indium
7 composition at the QD center is consistent with the targeted value of x_{In}. Interestingly, for the
8 multi-QD-template, STM reveals a mono-modal QD-size-distribution and a QD density of
9 $1.8 \times 10^{12}/cm^2$, higher than that for QD-template.

10 To consider possible mechanisms for the observed variations in QD densities, we estimate
11 the areal density of indium atoms in the top layer of QDs for each case. Using the QD densities
12 and sizes from STM, the local composition measurements from STS, and a linear interpolation of
13 lattice parameters, we estimate $\sim 1.0 \times 10^{15}$ indium atoms/cm^2, suggesting minimal surface
14 segregation of indium during the growth of the GaN capping layers. For multi-QD-template, the
15 QD nucleation is likely driven by the strain-fields from buried QDs, rather than the residual stress
16 surrounding threading dislocations. A similar increase in QD density with increasing number of
17 QD layers has been reported for multi-period InGaN/GaN QD SLs grown on free-standing GaN
18 substrates, further supporting the model for preferential QD nucleation at strain energy minima
19 directly above buried QDs.[18] Furthermore, calculations of the formation energy for indium clusters
20 on GaN suggest that biaxial strain impedes the formation of In-rich clusters, consistent with our
21 observed mono-modal QD-size-distribution in this case.[23] Since the InGaN wetting layer is
22 expected to be fully strained, the thickness and composition of the wetting layer are expected to
23 be independent of substrate. However, near threading dislocations, fluctuations in the wetting layer

ACCEPTED MANUSCRIPT

AIP Publishing

This manuscript was accepted by Appl. Phys. Lett. Click here to see the version of record.

thickness and/or composition may occur and are the subject of future investigations.

We now discuss the effective valence and conduction band edges (CBE), which presumably correspond to the lowest hole and highest electron confined states, E_h and E_e. For QD-free-standing, QD-template, and multi-QD-template, the values of E_e at the center of the InGaN QD are lower than those of the InGaN WL, as shown in Figs. 3(a), (b), and (c), respectively. In addition, the values of E_e are position-dependent, with the lowest value of E_e near the InGaN QD core, consistent with the higher effective x_{In} near the core, as discussed earlier.

For QD-free-standing, the values of E_e (E_h) as a function of the lateral and longitudinal distances across/between the QDs, indicated as x and y directions in Fig. 2(b), are presented as red dots (black squares) in Figs. 4(a) and 4(b), respectively. For comparison, local In composition profiles of similar-sized QDs[25,30] are converted to bandgap profiles using a quadratic interpolation of GaN and InN bandgaps, as described above. Based upon the energy bandgap profile and reported valence band offsets at InGaN/GaN heterojunctions,[24,31] we estimate the CBE and the valence-band edge (VBE) of a bulk-like InGaN alloy, shown as the dotted line guides-to-the-eye in Figs. 4(a) and 4(b). Similar to our measured values of E_h and E_e, the VBE is nearly constant with position, while the CBE decreases with position away from the QD centers.

For QD-template, shown in Fig. 3 (b), the larger difference between E_h values of the In-rich ultra-small QD and the InGaN WL suggest a valence band offset (VBO) which agrees well with the reported VBO of 0.58eV at the InN/GaN interface.[32] However, for the large QD, E_h and the resulting VBO is position-dependent, suggesting a complex interplay between strain and indium composition. For InGaN/GaN interfaces, first principles computations predict an increase in VBO for strained layers in comparison to those predicted for strain-relaxed layers.[33] Since the

ACCEPTED MANUSCRIPT

AIP Publishing

This manuscript was accepted by Appl. Phys. Lett. Click here to see the version of record.

QD diameter is the largest for QD-template, the strain variations across the QDs are likely more significant, resulting in the position-dependent VBO observed in this case.

In summary, we investigated the formation and electronic properties of InGaN QDs grown on free-standing GaN and GaN/sapphire templates, with and without buried InGaN/GaN QD SLs. For QD-free-standing, STM reveals a mono-modal QD-size-distribution, with the lowest density, consistent with a limited density of substrate threading dislocations serving as heterogeneous nucleation sites. For QD-template, STM reveals a bimodal QD-size-distribution, due to the nucleation of additional ultra-small InN-rich QDs near threading dislocations. For multi-QD-template, mono-modal QD-size-distributions with the highest QD density suggests that QD nucleation is enhanced by preferential nucleation at strain energy minima directly above buried QDs. For all cases, near the QD core, the effective band gaps are smallest and the effective conduction band offsets are largest, consistent with the predicted higher indium fractions at the QD core. For the moderately-sized QDs, the effective VBO is essentially independent of position, suggesting a minimal influence of the indium fraction. However, for the larger QDs, the effective VBO is position-dependent, presumably due to strain variations across the QD. This work opens up opportunities for tailoring the InGaN QD dimensions, densities, and electronic states by varying the starting substrate and the number of buried periods of QD SLs.

This material was based upon work supported by the National Science Foundation (NSF) through the Materials Research and Engineering Center at the University of Michigan, under grant No. DMR-1120923. J. C. Walrath and C. Greenhill were supported in part by the NSF Graduate Student Research Fellowship under Grant No. DGE 1256260. J. Occena was supported by NSF through grant No. DMR 1410282.

ACCEPTED MANUSCRIPT

AIP Publishing

This manuscript was accepted by Appl. Phys. Lett. Click here to see the version of record.

ACCEPTED MANUSCRIPT

1 # Figure Captions

2 **Fig. 1** Schematics of InGaN QD heterostructures for (a) single-layer InGaN QDs grown on free-
3 standing n^+ GaN (0001) substrates ("QD-free-standing"), (b) single-layer InGaN QDs grown on
4 GaN/AlN/sapphire templates ("QD-template"), and (c) three-period InGaN/GaN QD SLs grown
5 on GaN/AlN/sapphire templates ("multi-QD-template").

6 **Fig. 2** (a) Schematic and (b) large-scale STM image of QD-free-standing, as well as large-scale
7 STM images of (d) QD-template and (e) multi-QD-template. The images were acquired at a sample
8 bias voltage of -3.5 V; the grey scale ranges displayed are (b) 15 nm, (d) 8 nm, and (e) 5 nm,
9 respectively. The x and y axes in (b) correspond to the lateral and longitudinal directions in Fig. 4.
10 The QD diameter distributions for (c) QD-free-standing, (f) QD-template, and (f) multi-QD-
11 template are determined from an analysis of STM images. For (d) QD-template and (e) multi-QD-
12 template, example QDs are indicated with white arrows. The frequency is the percentage of QDs
13 with diameters within a specified range. Fits to a Gaussian distribution are shown as solid lines,
14 with χ values of (c) 0.84 and (f) 0.98 and 0.82. The maximum likelihood estimates of mean QD
15 diameters are (c) 17 ± 3 for QD-free-standing and (f) 5 ± 3 nm for multi-QD-template, calculated
16 from a total of (c) 35 and (f) 232 number of QDs, respectively. For QD-template, a bimodal
17 distribution of QD diameters is apparent, with most-probable values of 23 ± 1 nm and 3 ± 1 nm
18 for large and ultra-small QDs, respectively.

19 **Fig. 3** Plots of normalized conductance versus sample bias voltage, collected from the InGaN WL
20 and in the vicinity of InGaN QDs for (a) QD-free-standing, (b) QD-template, and (c) multi-QD-
21 template. For the InGaN WL, the solid-line spectra in (a) – (c) reveal well-defined band edges with
22 effective band gap values of 3.4 ± 0.1 eV, slightly larger than the anticipated effective bandgap of
23 the WL, presumably due to tip-induced band-bending.[24] Using a quadratic deviation from a linear

AIP Publishing

This manuscript was accepted by Appl. Phys. Lett. Click here to see the version of record.

1 interpolation of binary InN and GaN band gaps of 0.69 eV and 3.4 eV, with a bowing parameter
2 of 2.1 eV, the estimated x_{In} of 0.04 would lead to a band gap of 3.2 eV. Therefore, the local
3 bandgaps in the QD regions are estimated using a linear correction to effective bandgap values,
4 consisting of a multiplicative factor that would produce a WL bandgap of 3.2 eV. For all cases,
5 (a)-(c), the effective band gaps at the centers of the QDs are slower than those at the edges of the
6 QDs. For (b) QD-template, an effective band gap of 1.2 eV is attributed to an ultra-small QD
7 nucleated near threading dislocations.

8 **Fig. 4** For InGaN QDs from QD-free-standing, the confined hole energy, E_h, and the confined
9 electron energy, E_e, are plotted versus (a) the lateral distance, x, across a QD, and (b) the
10 longitudinal distance, y, between QDs. The x and y coordinates relative to the InGaN QD is shown
11 in Fig. 2(b). A position-dependence of E_e values is observed in both (a) and (b). For comparison,
12 local In composition profiles of similar-sized QDs[30] are converted to energy bandgap profiles using
13 a quadratic deviation from a linear interpolation of GaN and InN bandgaps, and the resulting
14 conduction band edges (CBE) and valence band edges (VBE) of a bulk-like InGaN alloy are shown
15 as the dotted line guides to the eye in both (a) and (b). Similar to the measured values of E_h and
16 E_e, the VBE is nearly constant with position, while the CBE decreases with position away from
17 the QD centers.

18

ACCEPTED MANUSCRIPT

AIP Publishing

This manuscript was accepted by Appl. Phys. Lett. Click here to see the version of record.

1 References

[1] S. Nakamura, M. Senoh, N. Iwasa, and S. Nagahama, *Jpn. J. Appl. Phys.* **34**, L797 (1995).

[2] S. Nakamura, M. Senoh, S. Nagahama, N. Iwasa, T. Yamada, T. Matsushita, Y. Sugimoto, and H. Kiyoku, *Appl. Phys. Lett.* **69**, 1477 (1996).

[3] E. T. Yu, X. Z. Dang, P. M. Asbeck, S. S. Lau, and G. J. Sullivan, *J. Vac. Sci. Technol. B* **17**, 1742 (1999).

[4] M. Zhang, P. Bhattacharya, and W. Guo, *Appl. Phys. Lett.* **97**, 011103 (2010).

[5] R. M. Farrell, E. C. Young, F. Wu, S. P.DenBaars, and J. S. Speck, *Semicond. Sci. Technol.* **27**, 024001 (2012).

[6] W. Guo, M. Zhang, A. Banerjee, P. Bhattacharya, *Nano Lett.* **10**, 3355 (2010).

[7] S. Schulz and E. P. O'Reilly, *Phys. Rev. B* **82**, 033411 (2010).

[8] T. Frost, A. Banerjee, K. Sun, S. L. Chuang, and P. Bhattacharya, *IEEE J. Quant. Electron.* **49**, 923 (2013).

[9] S. Pimputkar, J. S. Speck, S. P. DenBaars, and S. Nakamura, *Nature Photon.* **3**, 180–182 (2009).

[10] W. Ye, S. Hanson, M. Reason, X. Weng, and R. S. Goldman, *J. Vac. Sci. Technol. B* **23**,1736 (2005).

[11] J. Tersoff, C. Teichert, and M. G. Lagally, *Phys. Rev. Lett.* **76**, 1675 (1996).

[12] T. D. Moustakas, T. Xu, C. Thomidis, A. Y. Nikiforov, L. Zhou, and D. J. Smith, *Phys. Stat. Sol. (a)* **205**, 2560 (2008).

[13] P. Dłużewski, A.Belkadi, J. Chen, P.Ruterana, and G.Nouet, *Phys. Stat. Sol. (c)* **4**, 2403 (2007).

[14] T. Frost, A. Hazari, A. Aiello, M. Z. Baten, L. Yan, J. M. Millunchick, and P. Bhattacharya, *Jap. J. Appl. Phys.* **55**, 032101 (2016).

[15] T. Zhu, H. A. R. El-Ella, B. Reid, M. J. Holmes, R. A. Taylor, M. J. Kappers, and R. A. Oliver, *J. Cryst. Growth* **338**, 262 (2012).

ACCEPTED MANUSCRIPT

AIP Publishing

This manuscript was accepted by Appl. Phys. Lett. Click here to see the version of record.

[16] Ammono. "High-carrier-concentration n-type Ammono-GaN substrates" Ammono GaN Data sheets. Last modified September 06, 2011. https://www.ammono.com/files/products/Ammono_GaN_High-carrier-concentration_n-type_substrates_v_20110906.pdf.

[17] c-GaN bulk substrates were obtained from Ammono technologies.

[18] T. Frost, Ph.D. Thesis, University of Michigan, 2015.

[19] J. Moneta, M. Siekacz, E. Grzanka, T. Schulz, T. Markurt, M. Albrecht, and J. Smalc-Koziorowska, *Appl. Phys. Lett.* **113**, 031904 (2018).

[20] B. Lita, Ph.D. Thesis, University of Michigan, 2002.

[21] W. Zhao, L. Wang, W. Lv, L. Wang, J. Wang, Z. Hao, and Y. Luo, *Jap. J. Appl. Phys.* **50**, 065601 (2011).

[22] S. Haung, S. J. Kim, R. Levy, X. Q. Pan, and R. S. Goldman, *Appl. Phys. Lett.* **103**, 132104 (2013).

[23] H. Lei, J. Chen, and P.Ruterana, *J. Appl. Phys.* **108**, 103503 (2010).

[24] C. G. Van de Walle and J. Neugebauer, *Nature* **423**, 626 (2003).

[25] P. R. C. Kent, G. L. W. Hart, and A. Zunger, *Appl. Phys. Lett.* **81**, 4377 (2002).

[26] S. Pereira, M. R. Correia, T. Monteiro, E. Pereira, E. Alves, A. D. Sequeira, and N. Franco, *Appl. Phys. Lett.* **78**, 2137 (2001).

[27] V. Bougro, M. E. Levinshtein, S. L. Rumyantsev, A. Zubrilov, Eds. M. E. Levinshtein, S. L. Rumyantsev, M. S. Shur, John Wiley & Sons, Inc., New York **1**, (2001).

[28] R. J. Kashtiban, U. Bangert, B. Sherliker, M. P. Halsall, and A. J. Harvey, *J. Phys: Conf. Ser.* **209**, 012038 (2010).

[29] V. D. Dasika, R. S. Goldman, J. D. Song, W. J. Choi, N. K. Cho, and J. I. Lee, *J. Appl. Phys.* **106**, 014315 (2009).

[30] T. C. Wang, H. C. Kuo, T. C. Lu, C. E. Tsai, M. Y. Tsai, J. T. Hsu, and J. R. Yang, *Jpn. J. Appl. Phys*. **45**, 3560 (2006).

[31] G. Orsal, Y. El Gmili, N. Fressengeas, J. Streque, R. Djerboub, T. Moudakir, S. Sundaram, A. Ougazzaden, and J. P. Salvestrini, *Opt. Mater. Express* **4**, 1030 (2014).

ACCEPTED MANUSCRIPT

AIP Publishing

This manuscript was accepted by Appl. Phys. Lett. Click here to see the version of record.

[32] P. D. C. King, T. D. Veal, C. E. Kendrick, L. R. Bailey, S. M. Durbin, and C. F. McConville, Phys. Rev. B **78**, 033308 (2008).

[33] L. Dong, J. V. Mantese, V. Avrutin, Ü. Özgür, H. Morkoc¸ and S. P. Alpay, *J. Appl. Phys.* **114**, 043715 (2013).

ACCEPTED MANUSCRIPT

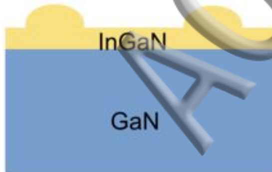

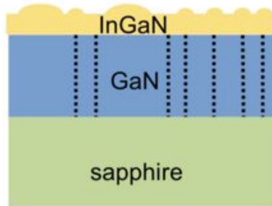

(c) multi-QD-template

InGaN

GaN

InGaN

GaN

InGaN

GaN

sapphire

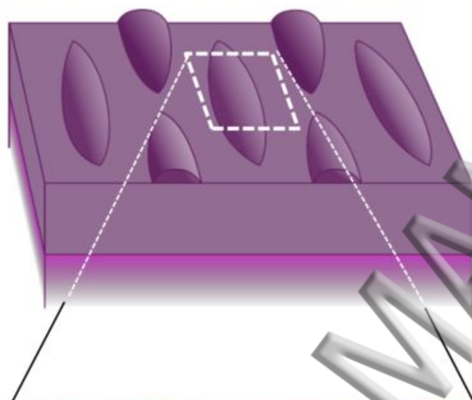

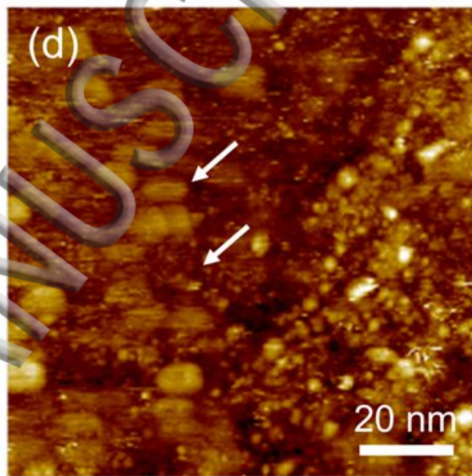

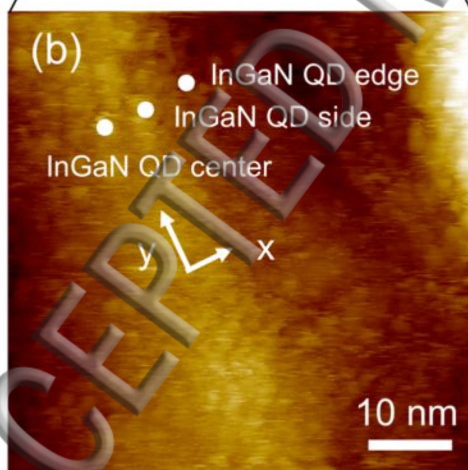

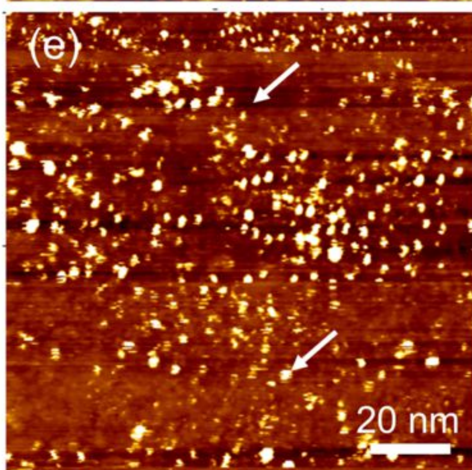

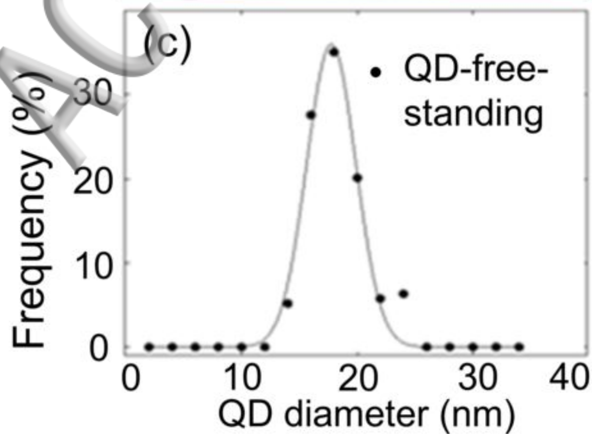

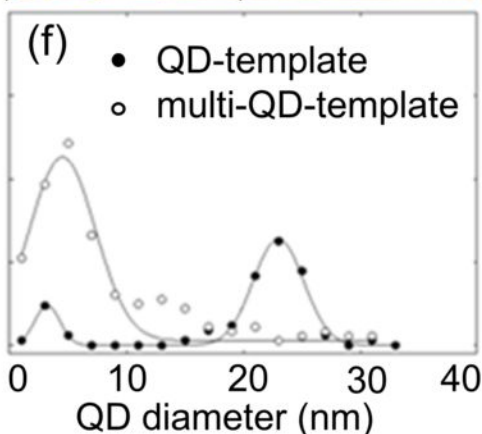

ACCEPTED MANUSCRIPT

This manuscript was accepted by Appl. Phys. Lett. Click here to see the version of record.

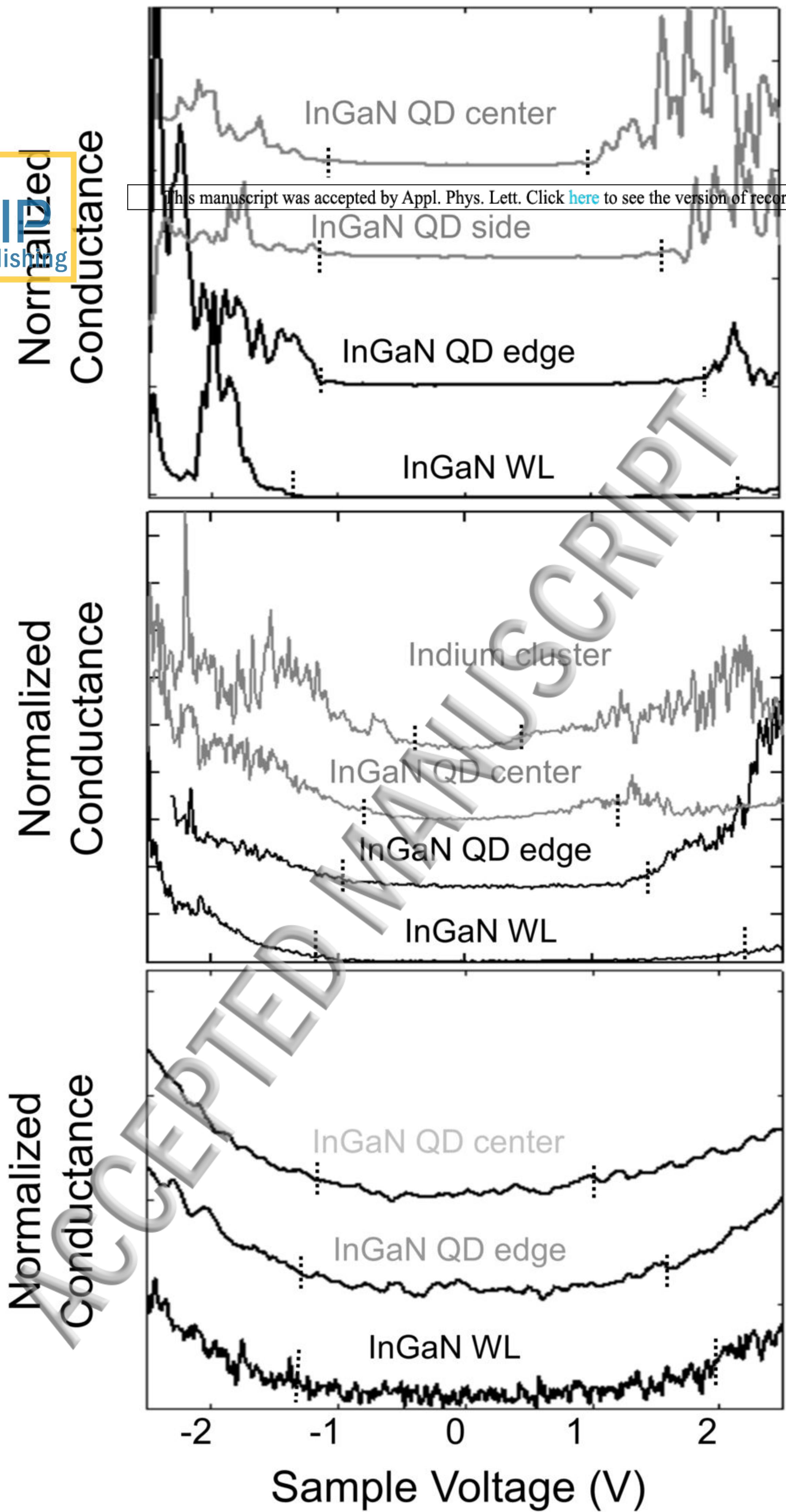

AIP Publishing

ACCEPTED MANUSCRIPT

AIP Publishing
This manuscript was accepted by Appl. Phys. Lett. Click here to see the version of record.
ACCEPTED MANUSCRIPT